Probability, not linear summation, mediates the detection of concentric orientation-defined textures

Gunnar Schmidtmann McGill Vision Research, Department of Ophthalmology, Montréal, Québec, Canada

Ben J. Jennings McGill Vision Research, Department of Ophthalmology, Montréal, Québec, Canada

Jason Bell School of Psychology, University of Western Australia, Crawley, Perth, Australia

Frederick A. A. Kingdom McGill Vision Research, Department of Ophthalmology, Montréal, Québec, Canada

Previous studies investigating signal integration in circular Glass patterns have concluded that the information in these patterns is linearly summed across the entire display for detection. Here we test whether an alternative form of summation, probability summation (PS), modeled under the assumptions of Signal Detection Theory (SDT), can be rejected as a model of Glass pattern detection. PS under SDT alone predicts that the exponent β of the Quick- (or Weibull-) fitted psychometric function should decrease with increasing signal area. We measured spatial integration in circular, radial, spiral, and parallel Glass patterns, as well as comparable patterns composed of Gabors instead of dot pairs. We measured the signal-to-noise ratio required for detection as a function of the size of the area containing signal, with the remaining area containing dot-pair or Gabor-orientation noise. Contrary to some previous studies, we found that the strength of summation never reached values close to linear summation for any stimuli. More importantly, the exponent β systematically decreased with signal area, as predicted by PS under SDT. We applied a model for PS under SDT and found that it gave a good account of the data. We conclude that probability summation is the most likely basis for the detection of circular, radial, spiral, and parallel orientation-defined textures.

Introduction

Whereas neurons in the early stages of cortical visual processing have small receptive fields and respond to only small regions of the visual scene, neurons in the higher processing stages tend to have larger receptive fields and respond to larger regions. A longstanding issue in visual science is thus: to what global properties of visual patterns are higher-stage neurons sensitive? In this communication we address this issue with respect to the global properties of concentric, orientation-defined textures, of which one form is the well-known Glass pattern.

Historically, neurons in the primary visual cortex (V1) were considered to act like filters tuned to orientation and spatial frequency (SF; Hubel & Wiesel, 1962; 1968). More recent work has revealed a more complex picture of nonlinear behavior that depends on stimulation from within, as well as from outside the classical receptive field, including contrast normalization, long-range interactions, surround suppression, and cross orientation inhibition (Carandini & Heeger, 2011; Loffler, 2008, for review). It has been suggested that beyond V1 the visual processing hierarchy follows two prominent pathways, the dorsal and the ventral stream (Goodale & Milner, 1992; Ungerleider & Mishkin, 1982), with the ventral stream mediating shape and form perception. Along the ventral stream, neurons in V2 and V4 are selectively responsive to more complex stimuli such as angles, arcs, and circles as well as hyperbolic and polar gratings (Anzai, Peng, & Van Essen, 2007; Gallant, Connor, Rakshit, Lewis, & Van Essen, 1996; Hegdé & Van Essen, 2007). Other studies have found cells in V4 tuned to stimuli with specific contour features, e.g., convex curvature, relative to the shape's center (Pasupathy & Connor, 1999; 2002; Yau, Pasupathy, Brincat, &

Citation: Schmidtmann, G., Jennings, B. J., Bell, J., & Kingdom, F. A. A. (2015). Probability, not linear summation, mediates the detection of concentric orientation-defined textures. *Journal of Vision*, *15*(16):6, 1–19, doi:10.1167/15.16.6.

doi: 10.1167/15.16.6 Received December 1, 2014; published December 7, 2015 ISSN 1534-7362 © 2015 ARVO

Downloaded From: http://jov.arvojournals.org/pdfaccess.ashx?url=/data/Journals/JOV/934737/ on 12/08/2015

Connor, 2012). In inferotemporal cortex (IT) neurons exist that are selective for complex shapes and objects such as faces (Desimone, Albright, Gross, & Bruce, 1984; Tanaka, 1996; Tsao & Livingstone, 2008).

These findings underscore the idea that the encoding of objects and shapes is accomplished by a hierarchical feedforward process along the ventral pathway (Cadieu et al., 2007; Serre, Kouh, Cadieu, Knoblich, & Kreiman, 2005; Serre, Oliva, & Poggio, 2007; Van Essen, Anderson, & Felleman, 1992). The question that arises is how local information detected in the early visual areas is integrated to encode more complex stimuli at subsequent stages.

Psychophysically, this has been tested in various ways. A popular approach is to determine the minimum number of signal elements required to detect the presence of a global pattern embedded in an array of noise elements. Such "coherence thresholds" have been used in a range of studies of motion (Braddick, O'Brien, Wattam-Bell, Atkinson, & Turner, 2000; Newsome, 1988), texture (Dakin, 1997; Wilson & Wilkinson, 1998; Wilson, Wilkinson, & Asaad, 1997), and contour perception (Achtman, Hess, & Wang, 2003; Braddick et al., 2000; Schmidtmann, Gordon, Bennett, & Loffler, 2013). Coherence thresholds in Glass patterns (Glass, 1969; Glass & Perez, 1973) have been employed to investigate signal integration in texture perception (Dakin, 1997; Dakin & Bex, 2002; Dickinson, Broderick, & Badcock, 2009; Wilson et al., 1997; Wilson & Wilkinson, 1998). Glass patterns are composed of an array of randomly positioned dot pairs, or "dipoles." The spatial relationship between dot pairs can be used to define the geometry of the global texture, e.g., circular, radial, parallel, etc., which cannot be detected on a purely local level. Current models of Glass pattern detection assume a two-stage process, in which the first stage extracts local orientation information while the second stage integrates the orientation information in order to extract the global stimulus structure (Wilson et al., 1997; Wilson & Wilkinson, 1998). This two-stage model is supported by physiological studies in macaques showing that neither the classical receptive fields nor surround mechanisms in early visual areas (V1, V2) are sufficient to process the Glass pattern's geometry (Smith, Bair, & Movshon, 2002; Smith, Kohn, Movshon, & Movshon, 2007).

A number of studies have suggested that the global structure in Glass patterns is processed by specialized detectors for circular and radial textures (e.g., Kelly, Bischof, Wong-Wylie, & Spetch, 2001; Kurki & Saarinen, 2004; Seu & Ferrera, 2001; Wilson et al., 1997; Wilson & Wilkinson, 1998). Some of these studies measured area summation for various types of Glass pattern, in which the stimulus array was subdivided into various sectors of increasing size. The linear summation prediction, which is that the decrease in threshold with increasing signal area follows a power-law function with a (log-log) slope of close to −1.0, was found only for circular Glass patterns (Wilson et al., 1997; Wilson & Wilkinson, 1998; cf. Dakin & Bex, 2002; Kurki, Laurinen, Peromaa, & Saarinen, 2003). Note, however, that a slope of −1.0 for linear summation is predicted only if the detection thresholds are expressed in terms of the proportion of signal elements within the signal sectors; if expressed in terms of the total number of signal elements, a slope of −1.0 would not be predicted. Furthermore, at least under the framework of Signal Detection Theory (SDT; see the following material), linear summation only predicts a slope of −1.0 in experiments where extrinsic uncertainty is introduced, either by employing an interleaved design or by randomly designating the angular orientation or "clock position" of the sectors containing the signal. The latter method has been employed in the experiments described here. If, on the other hand, a blocked design is employed, an optimal observer will benefit from using smaller integration windows that are matched to the signal area. In this case, linear summation predicts a slope of −1/2, owing to the summation of noise variances. The near −1.0 slopes observed in previous studies (Wilson et al., 1997; Wilson & Wilkinson, 1998; cf. Dakin & Bex, 2002; Kurki et al., 2003) were taken as psychophysical evidence for the existence of specialized global detectors for circular Glass patterns. In keeping with these results, it has been suggested that the Glass pattern's global structure is encoded in higher extrastriate areas (e.g., V4) by neurons with relatively large receptive fields, ones also selectively responsive to complex stimuli such as polar and hyperbolic gratings (Anzai et al., 2007; Gallant et al., 1996; Hegdé & Van Essen, 2007). Also in keeping are electrophysiological and imaging studies that demonstrated neural responses to radial and circular Glass patterns in V4 and LOC (Ostwald, Lam, Li, & Kourtzi, 2008; Pei, Pettet, Vildavski, & Norcia, 2005).

However, it is important to bear in mind that in some of these studies the measured summation slopes were much lower than predicted by linear summation (Dakin & Bex, 2002; Kurki et al., 2003; see Discussion for details). In spite of this, probability summation (PS) was not considered as a possible explanation for the weaker summation.

The model of PS that one might wish to test here is critical. Most studies on area summation have used PS models based on High Threshold Theory (HTT; e.g., Bell & Badcock, 2008; Dickinson, Han, Bell, & Badcock, 2010; Dickinson, McGinty, Webster, & Badcock, 2012; Loffler, Wilson, & Wilkinson, 2003; Meese & Williams, 2000; Morrone, Burr, & Vaina, 1995; Mullen, Beaudot, & Ivanov, 2011; Schmidtmann, Kennedy, Orbach, & Loffler, 2012; Tan, Dickinson, & Badcock, 2013). There is, however, considerable support for the idea that HTT is not a good model of PS and that SDT is preferable (Green & Swets, 1988;

Downloaded From: http://jov.arvojournals.org/pdfaccess.ashx?url=/data/Journals/JOV/934737/ on 12/08/2015

Laming, 2013; Nachmias, 1981; Shimozaki, Eckstein, & Abbey, 2003; Tyler & Chen, 2000). This raises the question of whether PS modeled according to SDT can be rejected for area summation in circular textures.

The aim of this study is to measure signal integration for a variety of Glass pattern and Glass-pattern-like textures and to test whether the results accord with probability or additive (of which a special case is linear) summation. To do this we have not only measured thresholds, but also the exponent β in the Quick-fitted psychometric functions. The exponent β, which is estimated from the fit to the data when the units of stimulus intensity are "raw" i.e., linear units, is related to the slope, or "steepness" of the psychometric function, in that β characterizes the slope when the units of stimulus intensity are plotted logarithmically spaced, as shown later (see Discussion for an analysis of the relationship between β and other measures of psychometric function slope; Strasburger, 2001). Historically β has been, and continues to be widely employed as a psychometric slope parameter for modeling PS under both HTT and SDT (e.g., Bell & Badcock, 2008; Loffler et al., 2003; Meese & Summers, 2012; Meese & Williams, 2000; Morrone et al., 1995; Schmidtmann et al., 2012; Tan, Bowden, Dickinson, & Badcock, 2015; Tan et al., 2013; Tyler & Chen, 2000; Watson, 1979). To avoid any confusion however with psychometric function "steepness," we will refer to β as the "exponent" of the psychometric function.

We measured β as a function of signal area under conditions in which subjects were unaware of the position of the signal sector, such that extrinsic uncertainty decreased with signal area. Assuming that intrinsic uncertainty is sufficiently low that our manipulation of extrinsic uncertainty has a meaningful impact on overall uncertainty, PS under SDT predicts a decrease in β with increasing signal area because of the resulting decrease in overall uncertainty (Kingdom, Baldwin, & Schmidtmann, 2015; Meese & Summers, 2012; Pelli, 1985; Tyler & Chen, 2000), whereas PS under HTT predicts no change in β (Mayer & Tyler, 1986). A failure to find such decreases in β would therefore constitute a valid basis for rejecting PS under SDT as a model for the detection of textures. This would leave open the possibility that either additive (including linear) summation, or probability summation under HTT is the correct model of detection.

Methods

Subjects

Five psychophysically experienced observers participated, three of the authors (BJJ, GS, and JB) and two observers who were naïve as to the purpose of the study. All observers had normal or corrected-to-normal visual acuity. Informed consent was obtained from each observer, and all experiments were conducted in accordance with the Declaration of Helsinki.

Apparatus

The stimulus patterns were generated using MATLAB (MATLAB R 2013a, MathWorks, Natick, MA) and presented on a gamma-corrected iiyama Vision Master Pro 513 CRT monitor (Iiyama, Nagano, Japan) running with a resolution of 1024×768 pixels and a frame rate of 85 Hz (mean luminance 38 cd/m^2), under the control of an Apple Mac Pro (3.33 GHz). Observers viewed the stimuli at a distance of 120 cm. At this distance one pixel subtends 0.018° of visual angle. Experiments were performed in a dimly-illuminated room. Routines from the Psychophysics Toolbox were employed to present the stimuli (Brainard, 1997; Pelli, 1997).

Procedure

All experiments were carried out under binocular viewing conditions. Observers completed short practice runs prior to data collection. Using a 2-IFC paradigm with the method of constant stimuli, the observer's task was to detect which of two successively presented stimulus arrays contained the target texture. One of the stimuli contained a variable fraction of oriented signal elements (see the following material) distributed within the signal area, the other contained noise only (randomly oriented Gabors or dot-pairs). The stimuli were presented on a midgray background. A trial consisted of the first stimulus being presented for 500 ms, followed by a 300-ms blank inter-interval delay (midgray blank screen), followed by the second stimulus (order of stimulus presentation randomized). In order to investigate the influence of a shorter presentation time used in some previous studies on Glass pattern detection, we conducted a control experiment where the stimulus presentation time was decreased to 160 ms (see Experiment 4). After the second interval the observer was presented with the blank midgray screen again and were then free to submit their answer via a key press, if they were unsure they were instructed to guess. If an incorrect answer was submitted a short beep was heard. The key press initiated the next trial. Ten different signal-to-noise ratios were presented 20 times in each experimental block in random order, resulting in 200 trials per sector size/arrangement condition. Different sector sizes and texture types were tested in a block design. Detection

Downloaded From: http://jov.arvojournals.org/pdfaccess.ashx?url=/data/Journals/JOV/934737/ on 12/08/2015

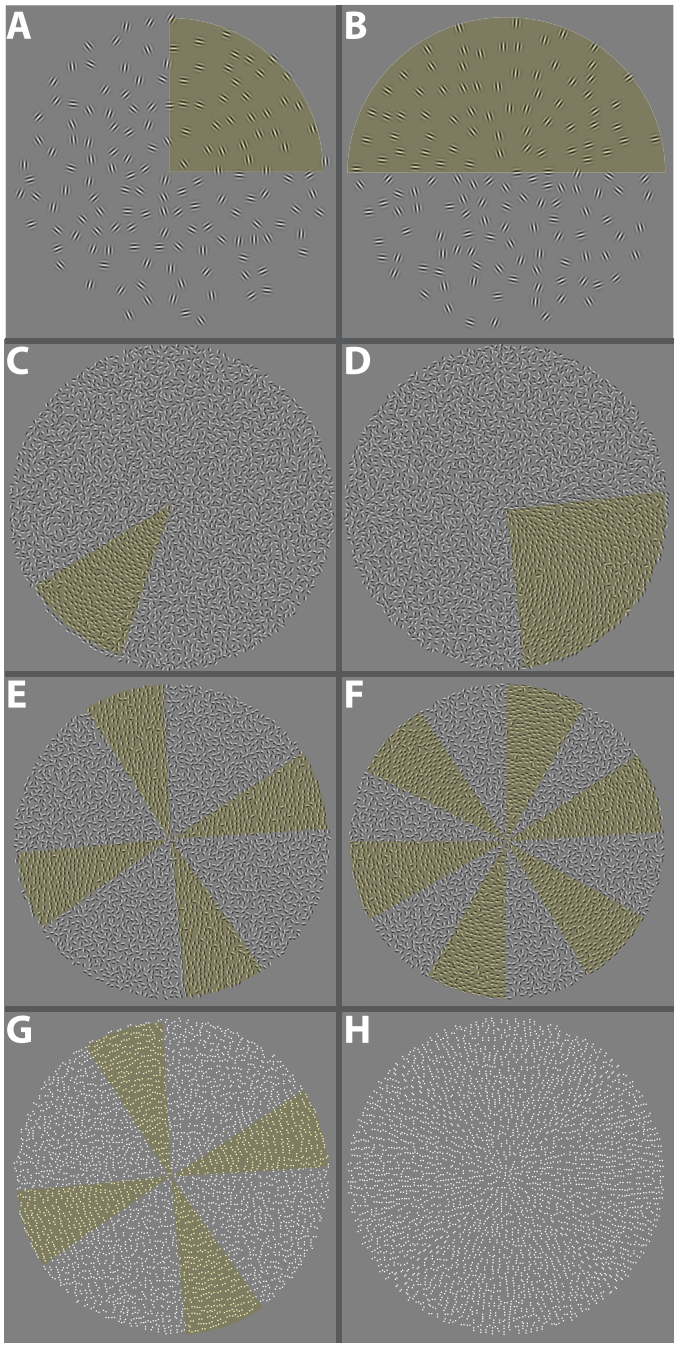

Figure 1. Stimulus examples. For illustration purposes the pie-wedges containing the signals are shaded in yellow. Integration strength was determined by measuring detection thresholds as a function of signal area. (A and B) Experiment 1 (Low-density) the stimulus was composed of 150 Gabor patches. The signal elements were restricted to a single pie-wedge shaped sector of varying angular size ranging from 36° to 360°, corresponding to signal areas ranging from 10% to 100% [A: circular 25% signal area (90°); B: radial 50% signal area (180°)]. (C and D) Experiment 2 (High-density) the total number of elements was increased to 3,000 to create a high density texture. The signal areas tested were 36°, 90°, 180°, and 360°, corresponding to 10%, 25%, 50%, and 100% signal areas [C: circular 10% signal area (36°); D: spiral 25% signal area (90°)]. (E and F) Experiment 3 (lower panel) the stimulus was composed of 3,000 Gabor elements; the signal elements were distributed in various pie-wedge configurations extending over the entire array similar to previous studies using Glass patterns. Detection thresholds were measured for 33%, 50%, and 100% signal area. For 33% signal area the signal elements were distributed across four pie-wedge sectors with an angular extent of 30° each, the 50% signal area stimulus had the signal elements distributed between six pie-wedges each with an angular extent of 30° [E: parallel 33% signal area (30°); F: circular 50% signal area (30°)]. (G and H) Glass patterns. The sector size and design was identical to Experiment 4: Detection thresholds were measured for 33%, 50%, and 100% signal area and for circular, radial, spiral, and parallel Glass patterns, where the signal elements were distributed in four or six pie-wedge shaped sectors. G: circular 33% signal area (30°); H: radial 100%. Note that all stimulus examples are shown with high signal-to-noise ratios.

thresholds are defined as the ratio of signal-to-noise elements in the signal areas of the texture. For instance, a detection threshold of 0.5 means that 50% of the elements (Gabors or dot-pairs) distributed throughout the signal area (pie-wedge sector/s) had to be oriented according to a texture type (circular, radial, spiral, or parallel) in order to detect the texture.

Stimuli

The texture stimuli were polar arrays of oriented Gabor patches or dot-pairs. The stimulus arrays were circular with a diameter of 500 pixels, which in a viewing distance of 120 cm subtended 9.2°. The overall stimulus size was the same as in Experiments 1–4. In all experiments signal integration was determined by measuring detection thresholds (signal-to-noise ratios) as a function of signal area. The angular position (clock-position) of the single or windmill-shaped pie-wedge sectors was randomized on each trial in all experiments with the exception of a control experiment, where the orientation was fixed at 90° (see Experiment 1). Example stimuli are shown in Figure 1. For illustration purposes, the pie-wedges containing the signals are shaded in yellow.

Experiment 1: Low-density textures

The Low-density texture stimuli in Experiment 1 contained 150 Gabor elements with a spatial frequency of 6 c/°. The circular-symmetric Gaussian envelope of the odd-symmetric Gabor patches had a standard deviation of 0.08°. Detection thresholds were

Downloaded From: http://jov.arvojournals.org/pdfaccess.ashx?url=/data/Journals/JOV/934737/ on 12/08/2015

measured for four different texture types: (a) circular, (b) radial, (c) spiral, and (d) parallel. The signal elements were oriented according to the texture type and noise elements were randomly oriented. The signal elements in the radial texture pattern were oriented such that their alignments converged on the center of the texture array. The signal elements in the circular textures were aligned tangentially to the array's radius. The orientation of the signal elements in the spiral texture varied as a function of the radial distance from the center of the array, such that the orientations of the elements at the center and the edge of the array differed by 60°. The orientation of the signal elements in the parallel texture was fixed at 90° (vertical). The position of the Gabors was randomly determined given the following conditions: In the Low-density stimulus the elements were forbidden from overlapping, In Experiment 1 detection thresholds were measured for signal areas of 10%, 12.5%, 16.67%, 25%, 32%, 37.5%, 50%, 62.5%, 75%, and 100%, which corresponded to angular extents of the single pie-wedge sectors of 36°, 45°, 60°, 90°, 115°, 135°, 180°, 225°, 270°, and 360°, respectively. Example stimuli are shown in Figure 1A and B.

Experiment 2: High-density textures

In order to investigate the influence of density, the number of Gabor elements was increased from 150 to 2,000 for Experiment 2 (High-density texture). The spatial frequency for these elements was 10 c/°. The Gaussian envelope of the center-symmetric Gabor patches had a standard deviation of 0.034°. A small overlap of 0.074° (~4 pixels) was tolerated in order to produce tight packing. The signal elements were restricted to one pie-wedge shaped sector. In Experiment 2 the signal areas tested were 10%, 25%, 50%, and 100%, which corresponded to angular extents of 36°, 90°, 180°, and 360°. Example stimuli are shown in Figure 1C and D.

Experiment 3: Windmill

In Experiment 3 the signal elements (2,000; same density as in Experiment 2) were distributed in various pie-wedge shaped sectors extending over the entire array, similar to previous studies using Glass patterns (Wilson et al., 1997; Wilson & Wilkinson, 1998). Detection thresholds were measured for 33%, 50%, and 100% signal area. For the 33% signal area condition the signal elements were distributed among four pie-wedge sectors each with an angular extent of 30°, forming a Maltese-cross-like stimulus. For the 50% signal area condition the signal elements were distributed among six pie-wedges each with an angular extent of 30°. Every second sector contained noise only. Example stimuli are illustrated in Figure 1E and F.

Experiment 4: Glass patterns

The Glass patterns used in Experiment 4 were similar to those used previously (Dakin & Bex, 2002; Wilson et al., 1997; Wilson & Wilkinson, 1998). They were composed of 3,000 white dot-pairs, with each dot measuring 2×2 pixels ($0.036° \times 0.036°$). The dot separation was set to 4 pixels (4.5′, 0.075°). Wilson and Wilkinson (1998) measured detection thresholds for various dot separations ranging from 4.5′ to 13′ and their results show that sensitivity is independent of density. Given the pixel size and dot separation, the Glass pattern design enabled eight different orientations of the dot pairs (0°, 30°, 45°, 60°, 90°, 120°, 135°, & 150°). Dot overlap was not allowed. Analogous to Experiment 3, detection thresholds were measured for 33%, 50%, and 100% signal area and for circular, radial, spiral, and parallel Glass patterns, where the signal elements were distributed in four or six pie-wedge shaped sectors. Example stimuli are shown in Figure 1G and H.

Data analysis

Percent correct responses were calculated and the resulting data fitted with a Quick function (Quick, 1974) using a custom-routine maximum-likelihood procedure based on binomial proportions, using MatLab's *fminsearch* function. The Quick function is:

$$F(x;\alpha,\beta) = 1 - 0.5 \cdot 2^{\left(-\left(\frac{x}{\alpha}\right)^{\beta}\right)} \quad (1)$$

where x is the proportion of signal elements within each signal sector, α is the proportion of signal elements (Gabors or dot-pairs) within each sector required for 75% correct detection, and β is the exponent that is related to the slope of the function.

Results

Experiment 1: Low-density textures

With the Low-density textures, the area of the single signal sector ranged from 10% to 100% of the entire stimulus. Detection thresholds α and exponents β were estimated from the psychometric functions of proportion correct as a function of proportion of signal elements. Thresholds were measured for circular, radial, spiral, and parallel textures. The results are presented in Figure 2, where the left most graph shows

Downloaded From: http://jov.arvojournals.org/pdfaccess.ashx?url=/data/Journals/JOV/934737/ on 12/08/2015

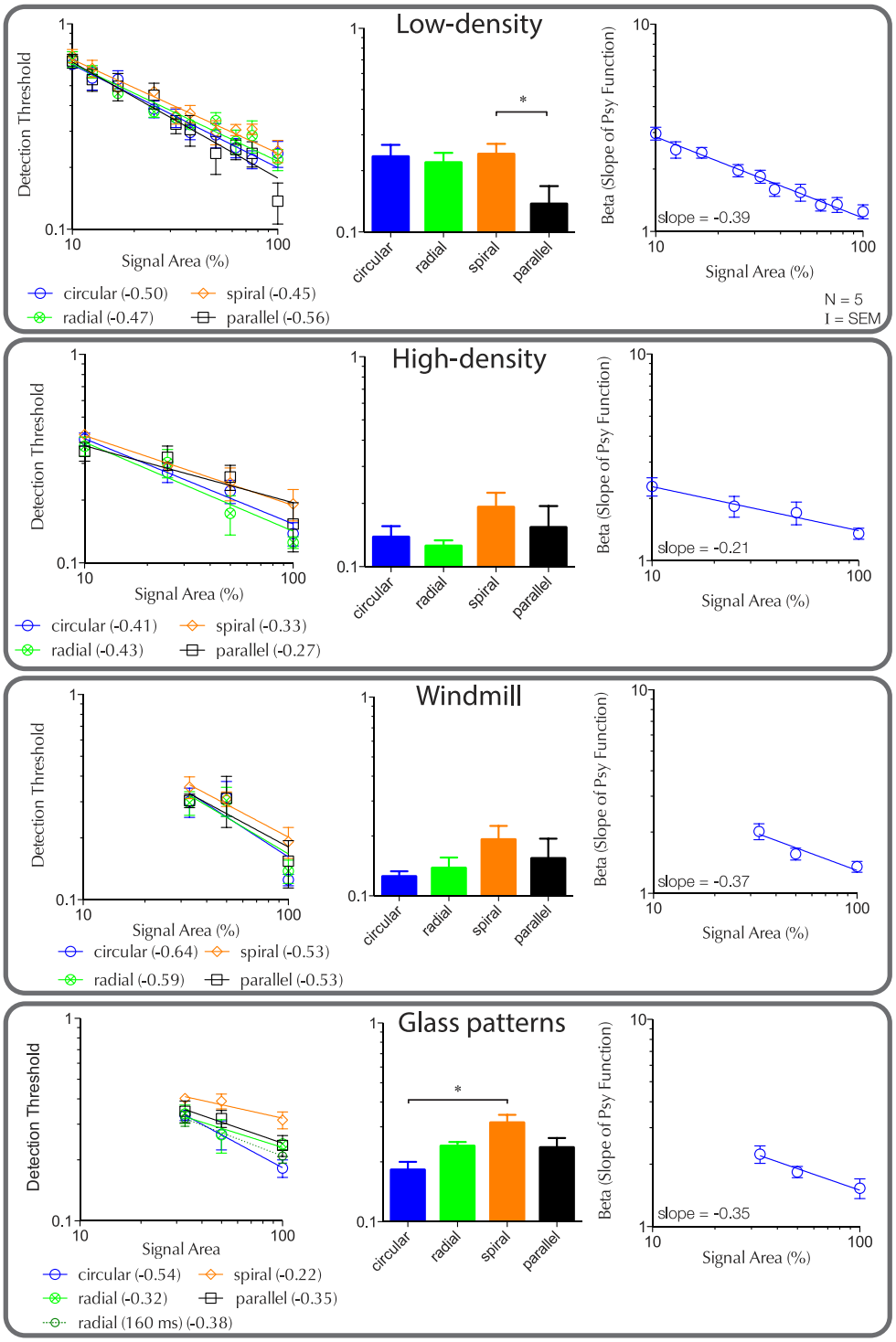

Figure 2. Detection thresholds (α) and exponents (β) as a function of signal area for four different texture types: circular (blue circles), radial (green circles), spiral (orange diamonds), and parallel (black squares). The left graphs show detection thresholds as a function of signal area. Detection thresholds here and elsewhere are defined as the ratio of signal to noise elements in the signal areas of the texture. Thresholds are averaged across subjects. The graphs in the middle show the detection thresholds for 100% signal area (right most data point of graphs on the left). The graphs on the right show the average β values of the psychometric functions as a function of signal area. β values are averaged across subjects and texture type. The average slopes of the power-law functions for each texture type are provided in the brackets of the legend. The asterisk (*) indicates significant differences. Error bars here and elsewhere represent $\pm$ standard error of the means.

Downloaded From: http://jov.arvojournals.org/pdfaccess.ashx?url=/data/Journals/JOV/934737/ on 12/08/2015

detection thresholds α (averaged across all observers) for each texture type and the right most graph shows the values of β (averaged across observers and texture types), both as a function of the signal area size (percentage of total stimulus area).

Results show that thresholds decrease with increasing signal area according to a power-law function, which results in a linear relationship when plotted in log-log coordinates. The slope of the fitted power-law function provides information about the strength of summation. The individual slopes range from −0.45 for the spiral texture to −0.56 for the parallel texture. The average slope is −0.49 ($SEM \pm 0.024$). The strength of summation is about half as strong as reported by some investigators (Wilson et al., 1997; Wilson & Wilkinson, 1998), but not others (Dakin & Bex, 2002; Kurki et al., 2003; see Discussion). A two-way repeated-measures ANOVA with factors texture type and signal area showed a significant decrease in threshold with increasing signal area, $F(9, 36) = 71.87$, $p < 0.001$, but no difference between the different texture types, $F(3, 12) = 3.612$, $p = 0.108$. The interaction term was not significant, $F(27, 108) = 1.016$, $p = 0.455$.

The middle graph in Figure 2 shows the detection thresholds for 100% signal area (rightmost data points in left graph) for all tested texture types. The results were analyzed with a one-way ANOVA (within-subjects) with the texture types as factor, revealing a significant effect, $F(3, 12) = 8.237$, $p = 0.003$. Subsequent post hoc test (Bonferroni corrected, here and throughout) showed a significant difference only between spiral and parallel textures ($p = 0.025$). Performance is similar for circular, radial and spiral texture and tends to be best for parallel texture. This is contrary to previous results showing much better performance for circular Glass patterns (Wilson et al., 1997; Wilson & Wilkinson, 1998; cf. Dakin & Bex, 2002). The same studies also showed the poorest performance for parallel textures.

In a control experiment the clock position of the sector was fixed vertically (90°) and thresholds were measured for signal areas of 10% and 50% for radial and circular textures. Results show a small but not significant decrease in threshold for small segment sizes (10%), i.e., advantage gained through the reduction of spatial uncertainty. Hence, the resulting summation is even less strong (−0.42).

The rightmost graph in Figure 2 shows the average β values as a function of signal area. β values range from 2.97 ($SEM \pm 0.21$) for 10% signal area to 1.25 ($SEM \pm 0.097$) for 100% signal area. This translates to a decrease in β with signal area with a slope on a log–log plot of −0.39 ($SEM \pm 0.021$). The statistical treatment of the β values will be described later in the modeling section.

Experiment 2: High-density textures

Previous studies have tended to use very dense Glass patterns, for instance Dakin and Bex (2002) used 1,966 dot-pairs. In order to investigate if density affects summation strength, the number of Gabor elements per array area was increased to 3,000, which is even denser than the Glass patterns employed in previous studies (Dakin & Bex, 2002; Wilson et al., 1997; Wilson & Wilkinson, 1998).

Results in Figure 2 (High-density) show that detection thresholds decrease with increasing signal area following a power-law function with average slopes of −0.39 ($SEM \pm 0.035$). The summation slopes are even shallower than in the Low-density experiment and range between −0.27 for parallel textures to −0.43 for radial textures. A two-way repeated-measures ANOVA (within-subjects) with factors of texture type and signal area revealed a significant increase in performance with increasing signal area, $F(3, 12) = 81.97$, $p < 0.001$, but no significant difference between the four different texture types, $F(3, 12) = 1.711$, $p = 0.218$. No significant interactions were found, $F(9, 36) = 1.912$, $p = 0.082$.

In order to investigate whether the increased density has an effect on detection sensitivity, we statistically compared the sensitivity for the Low-density stimuli in Experiment 1with the High-density Experiment here for the four tested signal areas (10%, 25%, 50%, and 100%). Given that the statistical analysis showed no significant differences for the texture types in Experiments 1 and the High-density textures here, we combined the thresholds for each texture type. A two-way repeated-measures ANOVA was conducted with density (Low-density, High-density) and area (10%, 25%, 50%, and 100%) as factors. Results show a significant effect for density, $F(1, 19) = 81.881$, $p < 0.001$, and area, $F(3, 57) = 208.664$, $p < 0.001$. Subsequent post hoc tests showed significant differences between the two densities and for all signal areas. Increasing the density leads to a decrease in detection thresholds. The analysis revealed a significant interaction between density and area, $F(3, 57) = 31.055$, $p < 0.001$, which reflects an initial steeper decrease in thresholds with increasing area.

The bar plot summarizes the detection thresholds for 100% signal area for all texture types (High-density) and shows no statistically significant difference between these, $F(3, 12) = 1.449$, $p = 0.277$. The average β values range between 2.29 ($SEM \pm 0.23$) for 10% signal area and 1.352 ($SEM \pm 0.083$) for 100% signal area. Similar to the Low-density Experiment, β decreases with increasing signal area [slope = −0.21 ($SEM \pm 0.024$)], as predicted by PS under SDT (see Discussion and Figure 4).

Downloaded From: http://jov.arvojournals.org/pdfaccess.ashx?url=/data/Journals/JOV/934737/ on 12/08/2015

Experiment 3: Windmill design

Increasing the density for the Gabor textures led to lower thresholds, but the summation strength was not affected and is much less for both stimulus designs compared to previous studies using Glass patterns (Dakin & Bex, 2002; Wilson et al., 1997; Wilson & Wilkinson, 1998). One additional explanation for the differences in our results might be the way that the signal elements are distributed with the stimulus array. Previous studies in similar area summation experiments have used a stimulus design in which the array is split into several pie-wedge shaped sectors, evenly distributed to form a windmill-like configuration (Dakin & Bex, 2002; Morrone et al., 1995; Wilson et al., 1997; Wilson & Wilkinson, 1998). Experiment 3 was conducted to investigate whether this difference in stimulus design could lead to such different results.

The stimulus design was similar to the one used by Wilson et al. (1997) and Wilson and Wilkinson (1998). In this design the signal elements were distributed between four (33% signal area) or six (50% signal area) sectors that were in turn arranged into the windmill-like pie-wedge sectors. The wedges between the signal areas contained randomly orientated noise elements. The 100% signal area was equivalent to the 100% signal area in Experiment 2. Similarly to the High-density stimuli in Experiment 2, the entire stimulus array was composed of 2,000 Gabor patches.

Results show that detection thresholds decrease with increasing signal area following a power-law function with slopes ranging between −0.53 for parallel and spiral textures to −0.64 for circular textures. The average slope is −0.57 ($SEM \pm 0.027$), consistent with the summation slopes measured in Experiments 1 and 2, but still only half the magnitude of the summation slopes reported previously (Wilson et al., 1997; Wilson & Wilkinson, 1998; cf. Dakin & Bex, 2002; Kurki et al., 2003). Similar to the Low-density and High-density stimuli, a two-way repeated-measures ANOVA revealed significant effect of signal area, $F(2, 8) = 34.918$, $p < 0.001$, but no significant difference in performance is as a function of texture type, $F(3, 12) = 1.02$, $p = 0.42$. No significant interaction was found. In a separate statistical analysis (one-way ANOVA) we compared the thresholds for the different texture types at 100% signal area. There is a tendency for a superior performance for circular textures, but the statistical analysis reveals no significant differences between the different textures, $F(3, 12) = 1.461$, $p = 0.274$.

The average β values range from 2.016 ($SEM \pm 0.182$) to 1.352 ($SEM \pm 0.083$). Similar to the results in Experiments 1 and 2, β decreases with increasing signal area, with a log–log slope of −0.37 ($SEM \pm 0.12$).

Experiment 4: Glass patterns

So far, all textures were composed of Gabor elements. One might argue that despite the efforts to match the Gabor textures to the Glass patterns used in previous studies, by increasing density (Experiment 2), fundamental differences remain and are responsible for the discrepancy between the results with previous studies (Dakin & Bex, 2002; Wilson et al., 1997; Wilson & Wilkinson, 1998). We therefore generated Glass patterns stimuli similar to those used by previous studies. Our results show that detection decreased with increasing signal area following a power-law function with slopes ranging from −0.22 for spiral to −0.54 for circular textures. The average slope, describing the increase in performance with increasing signal area, is −0.36 ($SEM \pm 0.067$), similarly shallow the Gabor textures in Experiment 3 (−0.37). A two-way ANOVA with texture type and area as factors revealed significant effects for both texture, $F(3, 12) = 11.00$, $p = 0.001$, and area, $F(2, 8) = 18.652$, $p = 0.001$. No significant interactions were found. Subsequent post hoc tests showed that detection thresholds for spiral Glass patterns were significantly higher compared to circular ($p = 0.001$) and radial Glass patterns ($p = 0.046$). In a separate one-way ANOVA we compared the detection thresholds for the different texture types for 100% signal area. The analysis showed a significant main effect, $F(3, 9) = 5.78$, $p = 0.017$. Additional post hoc tests showed that detection thresholds for circular Glass patterns were significantly lower than spiral ones ($p = 0.003$). Analyzing detection thresholds for Gabor textures at 100% signal area shows that performance is similar for circular, radial, and parallel Glass patterns. There is a bias towards a better performance for circular and radial Glass patterns, but these effects are not statistically significant. Furthermore, we compared detection thresholds for each texture type for the Gabor textures in Experiment 3 with the detection thresholds for Glass patterns with separate one-way ANOVAS. These revealed significant differences only between the spiral textures, $F(1, 3) = 16.18$, $p = 0.003$, showing that spiral Glass patterns are significantly harder to detect than spiral Gabor textures. Interestingly, there are no statistically significant differences between all the other Glass patterns and the Gabor textures, which suggests that the orientation information can be equally sufficiently extracted from dot pairs compared to oriented Gabors.

Some of the previous studies on Glass patterns used different (shorter) presentation times and this might account for the discrepancies between our and previous results. We therefore conducted a control experiment ($N = 5$) with a presentation time of 160 ms, which falls within the range of earlier studies (Dakin & Bex, 2002: 147 ms; Wilson et al., 1997: 167 ms; Wilson &

Downloaded From: http://jov.arvojournals.org/pdfaccess.ashx?url=/data/Journals/JOV/934737/ on 12/08/2015

Wilkinson, 1998: 167 ms). The results are presented in green dashed line and neither thresholds nor slopes are significantly different compared with the 500 ms data.

Most importantly, as in all experiments before, β decreases with increasing signal area, ranging from 2.24 ($SEM \pm 0.22$) for 33% signal area to 1.53 ($SEM \pm 0.16$) for 100% signal area. The average log–log slope of β as a function of signal area is −0.35 ($SEM \pm 0.061$).

Discussion

The aim of our experiments was to measure signal integration for a variety of Glass-pattern-like textures and to analyze the data in order to determine whether probability summation (PS) under the assumptions of signal-detection-theory (SDT) could be rejected as a model of detection. To this end we measured not only thresholds, but also the exponents of the psychometric functions β as a function of signal area. If the positions/orientations of the sectors containing the signals are randomized on each trial, as in all our experiments, PS under SDT predicts that β will decrease with signal area (Meese & Summers, 2012; Tyler & Chen, 2000). This was observed in all experiments. This is a novel result that has significant consequences for how we interpret increases in performance with signal area in textured stimuli.

Results: Detection thresholds

Before considering the psychometric slope data in more detail, it is important to compare our threshold data with that from previous studies using similar stimuli. Previous studies using circular Glass patterns have reported threshold versus signal area slopes of −1.0, as predicted by linear summation (Wilson et al., 1997; Wilson & Wilkinson, 1998; cf. Dakin & Bex, 2002; Kurki et al., 2003). Taken together with other evidence showing the highest detection sensitivities for circular textures and shapes (Achtman et al., 2003; Kelly et al., 2001; Kurki & Saarinen, 2004; Seu & Ferrera, 2001; Wilson et al., 1997; Wilson & Wilkinson, 1998) researchers have concluded that there exist specialized detectors for circular forms at intermediate stages of form processing. These detectors, it is argued, are composed of three processing stages: linear filtering of local orientation information (V1) followed by a full-wave rectification, local pooling by larger second-stage filters (V2), and finally global linear pooling by neurons in V4 (Wilson et al., 1997; Wilson & Wilkinson, 1998).

Irrespective of the actual underlying mechanisms, however, it is important to reiterate that only some of the observed summation slopes measured in these

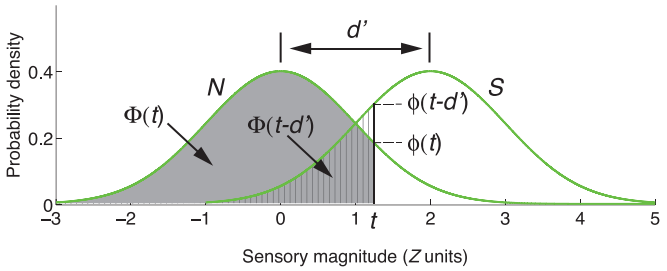

Figure 3. Parameters for calculating PS assuming SDT. N = noise distribution, S = signal-plus-noise distribution, d' = separation between S and N distributions. t is a sample sensory magnitude. $\Phi(t)$ and $\Phi(t\text{-}d')$ are the areas under the N and S distributions to the left of t. $\phi(t)$ and $\phi(t\text{-}d')$, are the heights of the N and S distributions at t. Reproduced from figure 3 in Kingdom, F. A. A., Baldwin, A. S., & Schmidtmann, G. (2015). Modeling probability and additive summation for detection across multiple mechanisms under the assumptions of signal detection theory. Journal of Vision, *15*(5):1, 1–16, doi:10.1167/15.5.1, with permission from the authors.

previous studies reached values close to linear summation. For example, Wilson and Wilkinson (1998) report much shallower summation slopes, on average −0.69, for radial and parallel Glass patterns (their figure 6). Wilson and Wilkinson account for these shallower summation slopes by assuming different weightings of the second stage of their model, resulting in predicted summation slopes of −0.74 i.e., close to their data. Dakin and Bex (2002) used a variety of signal geometries in their Glass patterns: For the circular patterns they employed a circular area whose radius was varied rather than the pie-wedge sector used here and by Wilson and colleagues; for the translational patterns, they used vertically oriented stripes as well as alternating annuli. We have replotted the rotational (circular) data from Dakin and Bex (2002; their figure 6 b–d), and find slopes on average of −0.48, which are much lower than −1.0 and indeed close to those measured here. For the translational patterns we find summation slopes of about −0.90 (their figure 6 e–g), which are similar to the ones found by Wilson and colleagues who used the pie-wedge sector design (Wilson et al., 1997; Wilson & Wilkinson, 1998). Kurki et al. (2003) measured spatial integration for circular Glass patterns as well as patterns with random dot-pair orientations (compared to random dot noise). They report much lower summation slopes for the concentric Glass patterns (−0.62) as well as the random-dot pair conditions (−0.48).

In none of our conditions do we find summation slopes close to linear summation, either for Gabor textures or Glass patterns. Our slopes are on average around −0.5 (low-density: −0.49; high-density: −0.36; windmill: −0.57; Glass patterns: −0.36). One might have supposed that the discrepancy between the Gabor

Downloaded From: http://jov.arvojournals.org/pdfaccess.ashx?url=/data/Journals/JOV/934737/ on 12/08/2015

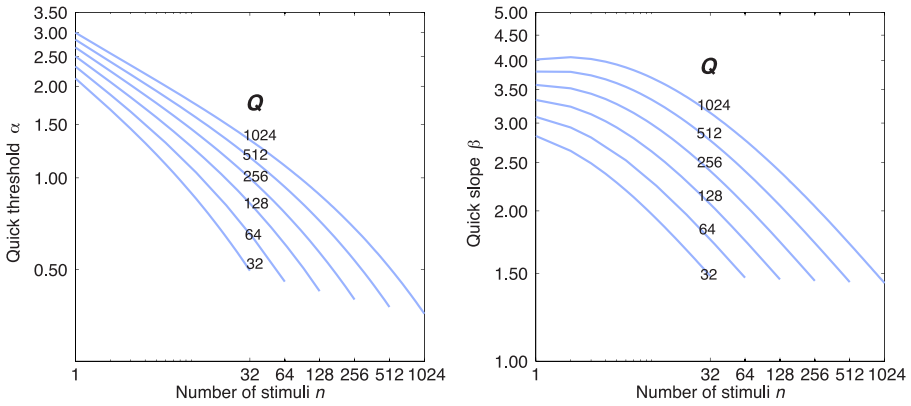

Figure 4. SDT PS predictions for Quick thresholds α (left graph) and β (right graph) as a function of the number of stimuli n, for different values of Q, the number of monitored mechanisms, ranging from 32 to 1,024. All predictions have been made for a system with a transducer exponent of $\tau = 1.125$ (the mean of the values used to fit the data in Figure 6) and for a $M = 2$-IFC task. Note the different logarithmic ranges on the ordinates of the two graphs.

textures we used and the Glass patterns of previous studies was due to the inherent differences in their stimulus structures, but our Glass pattern summation slopes were no steeper than our Gabor pattern summation slopes, and for various densities of the Gabor patterns. Or and Elder (2011) recently showed that sensitivity to Glass patterns increased by a factor of 1.8 when the dot pair was replaced with lines. However, we found no differences in sensitivity between Glass patterns and Gabor textures, with the exception of the spiral stimuli. It therefore remains somewhat of a mystery as to why the threshold versus signal area slopes found here are shallower than in previous studies, and why there is no difference in our study between the thresholds for Glass patterns and Gabor textures.

Also in contradiction to some previous studies is that we found no difference in sensitivities for detecting circular and radial structure (e.g., see Kelly et al., 2001; Kurki & Saarinen, 2004; Pei et al., 2005; Seu & Ferrera, 2001; Wilson et al., 1997; Wilson & Wilkinson, 1998). Some of our results show a tendency towards the hierarchy observed in previous studies, by which the detection thresholds were found to be lowest for circular texture, followed by radial, spiral, and parallel (see Figure 2). However, the differences were not significant except for the circular versus spiral Glass pattern condition in Experiment 4.

Wilson et al. (1997) report that detection thresholds for parallel Glass patterns are much higher (ranging from 3.5 to 5x, their figure 2) than circular Glass patterns. In contrast, our results for low-density textures (Figure 2, Low-density) show that the performance tends to be best for parallel textures (only in some cases the parallel textures elicited the lowest thresholds). In short, despite our best efforts to eliminate differences in stimulus design, density, and presentation time, we find detection sensitivities to be largely independent of texture type. As a reminder, there have been previous controversies over this issue. Dakin and Bex (2002) found that the advantage for circular Glass patterns was only evident if the stimulus was presented within a circular window: Most of their results (7/9) showed no superiority for circular structure and one subject even showed an advantage for translational (parallel) Glass patterns (see their figure 4).

Results: Exponent β

The main focus of this study was to analyze the data with respect to whether or not PS under SDT could be rejected as a model of area summation. The principal data for addressing this issue are the psychometric function β values, and, in particular, how they vary with signal area.

Previous studies on area summation experiments using stimuli other than Glass patterns have frequently applied PS models based on HTT (e.g., Bell & Badcock, 2008; Dickinson et al., 2010; Dickinson, Harman, Tan, & Almeida, 2012; Loffler et al., 2003; Schmidtmann et al., 2012; Tan et al., 2013). This model assumes a high threshold and therefore negligible false-positive responses. According to this model, thresholds fall with a power-law slope of $-1/\beta$ (Graham, 1989; Quick, 1974; Robson & Graham, 1981; Watson, 1979). A complete derivation from first principles of this model prediction can be found in Kingdom and Prins (2016). Most importantly, HTT predicts that β is constant across signal area, as also predicted by additive (including linear) summation models.

It is now generally accepted that SDT provides the most appropriate model to describe underlying decision processes observed in psychophysical experiments, whether those processes involve probability or additive summation (Green & Swets, 1988; Laming, 2013; Nachmias, 1981; Shimozaki et al., 2003; Tyler & Chen,

Downloaded From: http://jov.arvojournals.org/pdfaccess.ashx?url=/data/Journals/JOV/934737/ on 12/08/2015

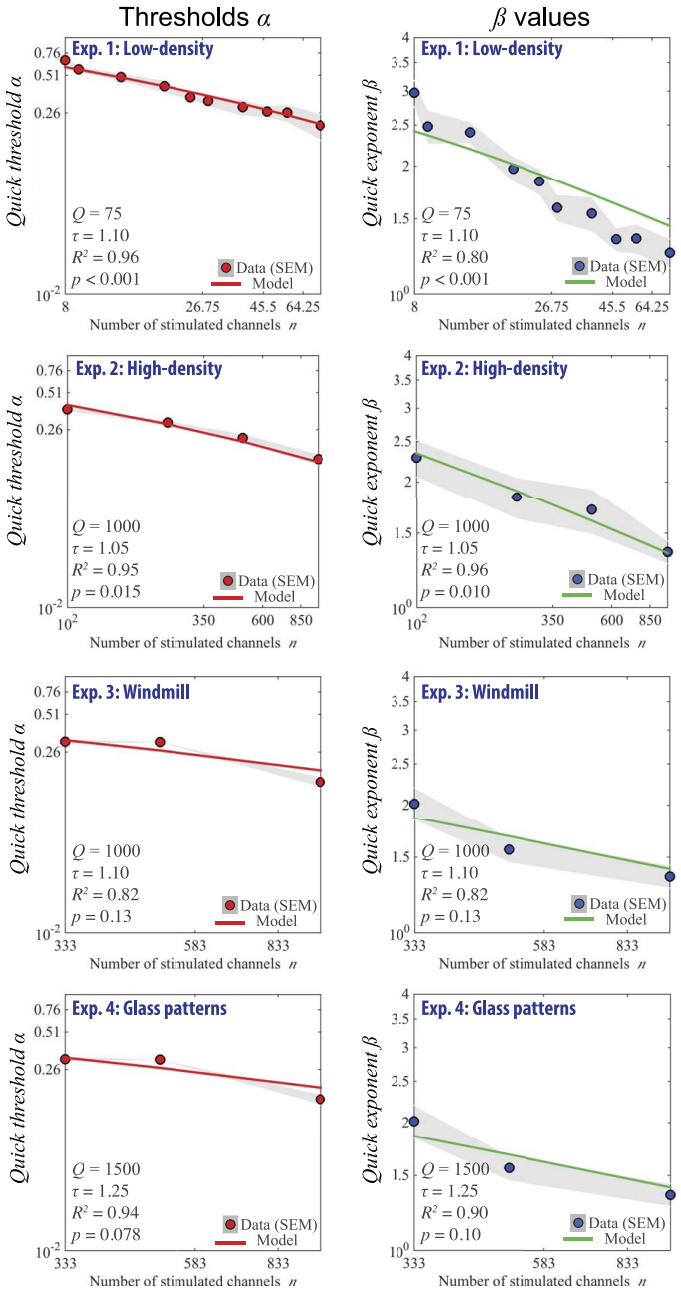

Figure 5. Predictions of the PS model under SDT set against the data. Left column: thresholds α: Right column: β. Threshold data are shown in red and β in blue. The shaded regions show $\pm$*SEMs*. Model predictions for α-*versus-n slopes* are shown by the red and for β-*versus-n slopes* by the green lines in each graph. The best-fitting exponent of the transducer function τ is indicated for each pair of graphs. No scaling was applied to the model prediction for β. The goodness of fit was evaluated by R^2, which is given in each graph. The *p*-value in each graph refers to the statistical significance of the correlation between the model predication and the observed data.

2000). In contrast to HTT, SDT alone predicts a dependence of β on stimulus uncertainty when the observer attends to all parts of the stimulus in which the signal might occur (Meese & Summers, 2012; Tyler & Chen, 2000). Our results consistently show that β decreases with signal area, i.e., as uncertainty decreases, as predicted by SDT. Although at a qualitative level our results are therefore consistent with PS under SDT, and not consistent with either PS under HTT, or additive (including linear) summation, we wanted to determine how quantitatively our data could be modeled by PS under SDT.

Probability summation model

The detailed mathematical derivation of the model in the following material is given in Kingdom et al. (2015). The model is a development of the standard SDT model for calculating proportion correct in *M*-AFC (*M*-IFC) tasks (Green & Swets, 1988; Kingdom & Prins, 2016), and generalizes the PS model of Shimozaki et al. (2003) to include the full gamut of relevant parameters. As is typical in SDT models, the noise-alone ("noise") and stimulus-plus-noise ("stimulus") intervals/locations are modeled as normal distributions with equal variance, with signal intensity given in Z, i.e., standard deviation units with respect to the center of the noise distribution. The separation of the two distributions is symbolized by d', which is thus a measure of the internal strength of the stimulus (Figure 3). The aim of the observer in a 2-IFC task is to identify on each trial the interval containing the target stimulus. The assumed strategy is the optimal decision rule: select the interval with the biggest signal. This is termed the MAX-rule.

The model is based on four quantities derived from the two distributions, as illustrated in Figure 3. If t is the intensity of a *sample* signal these are $\phi(t)$ and $\phi(t\text{-}d')$, which are the heights, or relative likelihoods of t in the noise and stimulus distributions, and $\Phi(t)$ and $\Phi(t\text{-}d')$, which are the areas of the noise and stimulus distributions below t. Kingdom et al. (2015) showed that when multiple stimuli are combined by PS, proportion correct (Pc) detection is given by the following:

$$Pc = n\int_{-\infty}^{\infty}\phi(t-d')\Phi(t)^{QM-n}\Phi(t-d')^{n-1}dt + (Q-n)\int_{-\infty}^{\infty}\phi(t)\Phi(t)^{QM-n-1}\Phi(t-d')^{n}dt \quad (2)$$

with

$$d' = (gs)^{\tau} \quad (3)$$

where M is the number of task intervals/alternatives (here 2), Q the number of monitored channels, n the

Downloaded From: http://jov.arvojournals.org/pdfaccess.ashx?url=/data/Journals/JOV/934737/ on 12/08/2015

Q	α-vs.-n slope 0–100%	α-vs.-n slope 10–100%	α-vs.-n slope 33–100%	β-vs.-n slope 0–100%	β-vs.-n slope 10–100%	β-vs.-n slope 33–100%
32	−0.44	−0.47	−0.51	−0.20	−0.23	−0.25
64	−0.39	−0.47	−0.53	−0.18	−0.24	−0.26
128	−0.36	−0.44	−0.50	−0.17	−0.24	−0.26
256	−0.33	−0.44	−0.49	−0.17	−0.24	−0.26
512	−0.31	−0.43	−0.49	−0.16	−0.25	−0.26
1,024	−0.29	−0.42	−0.48	−0.15	−0.25	−0.26

Table 1. Model α-versus-*n* and β-versus-*n* slope values from Figure 5, calculated for different *Q* values (32, 64, 128, 256, 512, 1,024) and for different ranges of *n*. Slope values are best fitting straight lines through the log-log data. The ranges of *n* are 0–100%, 10–100%, and 33–100%.

number of those channels containing stimulus (signal), τ the exponent of the transducer, s the intensity, or amplitude of the stimulus, and g a stimulus intensity scaling factor. Equation 2, which uses numerical integration, has been verified by Monte Carlo simulation, and is implemented by the routine PAL_SDT_PS_SLtoPC in the Palamedes Toolbox (Prins & Kingdom, 2009). The routine calculates proportion correct for any s, g, τ, M, Q, and n. Equation 2 can be thought of as an equation for a psychometric function, since it describes Pc as a function of stimulus strength s, given the parameters g, τ, Q, and n. It may be used therefore to *simulate* psychometric functions of Pc against s, which can then be fitted with a conventional psychometric function such as a Weibull or Quick function (Kingdom et al., 2015). That is how we have used it here. We employ Equation 2 to simulate psychometric functions, which are then fitted with Quick functions. This enables us to determine how Quick function parameters such as threshold α and exponent β vary with the parameters n, τ, and Q (see again Kingdom et al., 2015).

Before considering how well the PS model fares with our data, we provide an overview of how α and β in the Quick function would be expected to vary as a function of both Q and n, using simulated psychometric functions generated from the model as described above. To do this we set the scaling factor g to unity, M to 2 and the transducer exponent τ to 1.125, which we found to be the average value that best fitted the data, as described in the following material. Then, for each combination of Q and n, we used 30 equally-spaced values of s and generated a psychometric function that spanned the range 50% to 99.9% correct (less than 100% to avoid d' becoming infinity). Each function was then fitted by a Quick function and the threshold α and exponent β estimated.

Figure 4 shows how both α and β are predicted to decline with n for various values of Q. Table 1 presents the slopes of the decline when a straight line is fitted to portions of the log—log model data. As Table 1 shows, the modelled decline in α and β varies to some extent with Q as well as the range of n selected, with least variation across Q when only the upper 33% to 100% of n is selected.

We now apply the PS model to our data. Our approach is first to concentrate on the β values because for β there are only two free model parameters, the exponent on the transducer τ and the number of monitored channels Q (for α there are three free parameters, g, τ, and Q, where g is the stimulus intensity scaling factor). In the context of our stimuli and model, Q can be thought of as the number of independently-monitored regions of the stimulus. The model proposed here may be considered as a probability summation version of the model previously suggested for concentric Glass patterns (Wilson et al., 1997; Wilson & Wilkinson, 1998; Wilson & Wilkinson, 2015). This model consists of three processing stages: (1) First-stage local orientation filters, e.g., V1 simple cells, followed by a full-wave rectification, (2) pooling by larger second-stage filters in V2, and (3) global pooling across the whole stimulus by neurons in V4 (Wilson et al., 1997; Wilson & Wilkinson, 1998). Wilson and colleagues' second-stage filters, which act like end-stopped cells, are designed to extract local curvature (V2; see also Dobbins, Zucker, & Cynader, 1987; Wilson, 1999). Their responses are then linearly pooled by the third stage (V4). However, Wilson et al.'s (1997) model is conceivable without this intermediate stage, whereas in our model the stage is necessary to encode the local geometric arrangement of the elements (e.g., circular, radial, etc.) prior to the final probability summation stage. It is important to emphasize that the size of the putative second-stage filters, or the number and size of their first-stage inputs, is not specified in Wilsons (1997) model and, to our knowledge, there is no consensus from either psychophysics or physiology as to what their values might be. Hence, we can only speculate about the size of the second-stage filters and their degree of spatial overlap, and hence only speculate as to the precise value of Q, the number of monitored channels/filters. As in Wilson et al.'s model, we assume that the second-stage filters and their first-stage inputs are oriented to match the local parts of the stimulus. In other words, the visual system, even though it

Downloaded From: http://jov.arvojournals.org/pdfaccess.ashx?url=/data/Journals/JOV/934737/ on 12/08/2015

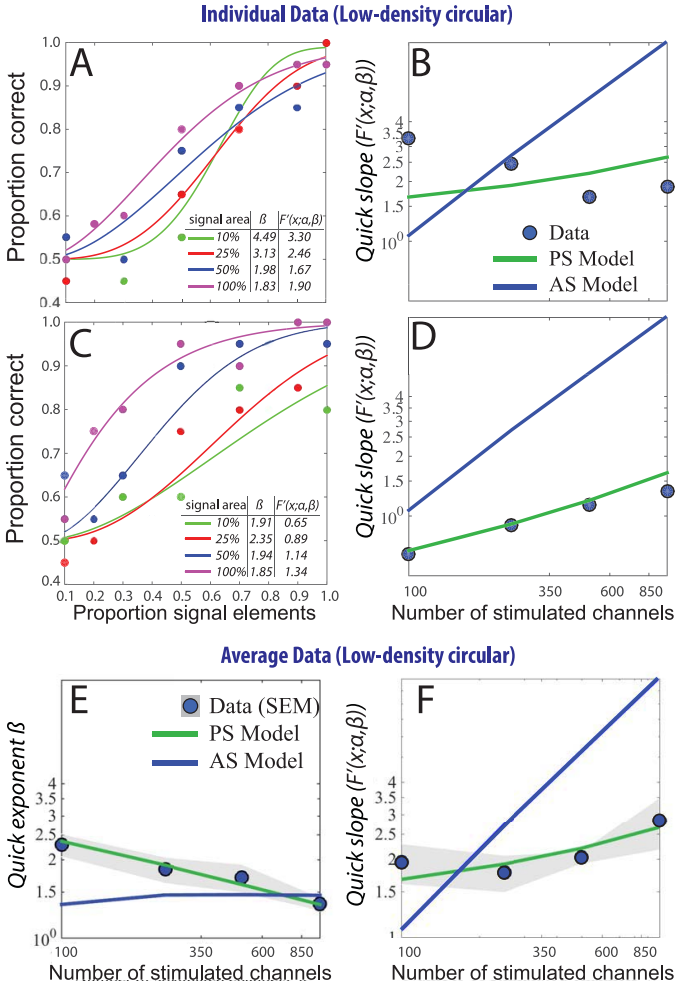

Figure 6. (A) shows individual psychometric functions for one subject for Experiment 2 (Low-density). The legend summarizes the Quick exponents β and the derivatives [$F'(x,\beta)$] for each signal area. (B) shows the data expressed as derivatives as a function of the number of stimulated channels n as well as the additive (blue line) and probability summation (green line) prediction to exemplify the relationship between β and the derivative. (C) and (D) show an example closer to the average data presented in Figure 5. (E) and (F) show the average exponent β and the derivatives of the Quick psychometric function across all subjects ($N = 5$) for Experiment 2 (Low-density textures) as a function of stimulated channels n. When data are expressed as derivatives, additive summation predicts a steep increase with increasing number of stimulated channels (blue line), whereas probability summation (green line) predicts a much shallower increase of the slope (derivatives).

probability summates the outputs of those second-stage filters via the MAX-rule, monitors the totality of filters that are matched to the particular stimulus arrangement (circular, radial, etc.). We initially explored various combinations of τ and Q to determine which combinations minimized the difference between model and data, but for nearly all conditions we were unable to find an optimum value of Q. The reason for this is that the observed β-versus-n slopes were in nearly all cases slightly steeper than the model β-versus-n slopes, whichever value of Q we tried (up to 5,000). It should be born in mind, however, that Q (unlike τ) has only a small effect on the absolute model values of β and a negligible effect on the β-versus-n slopes, as can be seen in Table 1. Despite the nondependency of the modeled results on Q, we have chosen to use different values of Q for each experiment. The values are chosen according to the number of Gabor elements or dot-pairs used in each stimulus. Specifically, Experiment 1 Low-density: Number of elements (NoE) = 150, $Q = 75$; Experiments 2 and 3 High-density and Windmill: NoE = 2,000, $Q =$ 1,000; Experiment 4 Glass patterns: NoE = 3,000, $Q =$ 1,500. Having set the value of Q, we then found the optimal value of τ for the β data, and used this value to predict the α-versus-n slopes (for which the stimulus scaling factor g is arbitrary). Note, however, that the fundamental difference between Wilson et al.'s (1997, 1998) Glass pattern model and our model is the final pooling stage of the second-level filters, which are pooled linearly in Wilson et al.'s model, but in our model summed by probability summation.

Figure 5 and Table 2 shows the results of this modeling exercise. In Figure 5, the model α values have been scaled vertically to fit the data—however, this does not affect the model's critical α-versus-n slopes. No scaling is applied to the β values. Figure 5 shows the model fits to the data as green lines, and Table 2 provides a comparison between model and data α-versus-n as well as β-versus-n slope values. Except for Experiment 2, the model slightly underestimates the decline of β with signal area but otherwise captures the decline in both α and β with increasing signal area very well. The goodness of fit between the model and the data was evaluated by calculating the coefficient of determination R^2 for each experiment, which is given for each graph in Figure 5. In order to validate the model predictions statistically, one-tailed significance probability values of the correlation coefficient R between data and model predictions for both α and β were calculated and p-values are stated in each graph of Figure 6. Note, that for four out of the eight conditions the $p < 0.05$ significance level is not reached owing to the fact that, in spite of the high correlation, the number of data points is only three (Figure 5E and F and Figure 5G and H, respectively). The small sample size is due to the reuse of the windmill stimulus design used in previous studies (Wilson et al., 1997; Wilson & Wilkinson, 1998), in order to enable consistent comparisons between studies.

It should be reiterated that the predictions are not critically dependent on the exact value of Q that we chose: Whatever value we had chosen, the decline in β with signal area would have been predicted, though slightly less well had we chosen smaller values of Q.

Downloaded From: http://jov.arvojournals.org/pdfaccess.ashx?url=/data/Journals/JOV/934737/ on 12/08/2015

Experiment	Data α-vs.-n slope	Model α-vs.-n slope	Data β-vs.-n slope	Model β-vs.-n slope
1.	−0.49 (*SEM* ± 0.024)	−0.47	−0.39 (*SEM* ± 0.021)	−0.23
2.	−0.39 (*SEM* ± 0.035)	−0.45	−0.21 (*SEM* ± 0.024)	−0.24
3.	−0.57 (*SEM* ± 0.027)	−0.48	−0.37 (*SEM* ± 0.12)	−0.26
4.	−0.36 (*SEM* ± 0.057)	−0.48	−0.35 (*SEM* ± 0.061)	−0.26

Table 2. Comparison between data and model α-versus-n and β-versus-n slope values and Table 1. The ranges of n are 10–100% for Experiments 1 and 2, and 33–100% for Experiments 2 and 3.

Model predictions for psychometric function slopes measured as derivatives

In addition to the analysis of the exponent β, we have also analyzed model predictions with respect to the derivative of the psychometric function (see Strasburger, 2001, for an analysis of the relationship between β and other measures of psychometric function slope). The derivative of the Quick function is:

$$F'(x;\alpha,\beta) = (1-\gamma)\cdot 2^{\left(-\left(\frac{x}{\alpha}\right)^{\beta}\right)}\cdot \left({}^{x}/_{\alpha}\right)^{\beta-1}\cdot\frac{\beta}{2} \quad (4)$$

Figure 6A shows individual psychometric functions for one observer for Experiment 1 (Low-density). The legend summarizes the values of β and the derivatives of the psychometric functions. Note that for this observer β drastically decreases with increasing signal area (β ranges from 4.49–1.83). However across observers, the average decline in β (see Figure 5 and graphs in left column of Figure 2) is more subtle (Experiment 1 β; range: 2.97–1.25; Experiment 2: 2.29–1.352; Experiment 3: 2.016–1.55; Experiment 4: 2.24–1.53). The extreme subject's decline in β leads to the decrease in slopes as measured by the derivative of the psychometric functions, despite the fact that our model predicts an increase in the derivatives. Figure 6 shows plots of the derivatives of the extreme subject case (6B), a more typical subject case (6D), and the average of the derivatives across subjects ($N = 5$; 6F) for this condition, with each plot also showing the AS and PS predictions of our model.

According to Kingdom et al. (2015) additive summation (AS) for stimulus components of equal strength is defined as:

$$d' = \frac{n(gs)^{\tau}}{\sqrt{Q}} \quad (5)$$

Note that for the derivatives the AS prediction is a very steep increase with increasing number of stimulated channels (blue line), whereas the PS (green line) prediction is a much shallower increase. Despite the slight decrease in the derivatives in the extreme subject's case (6B), PS still provides a much closer fit to the observed data than does AS. The fit is closer still for the derivatives for the typical (6D) and average (6F) cases. The bottom left figure in the plot shows average data and model predictions for the exponent β.

In summary, despite the decrease in the derivatives with increasing number of stimulated channels in the extreme subject's case, PS fits the data for this subject far better than does AS, and better still for the typical subject and average subjects' data. Hence, the SDT PS model accounts for the data better than the SDT AS model, even when based on an analysis of the steepness (derivative) of the psychometric function.

An alternative explanation: Matched linear filters?

Meese (personal communication) has suggested an alternative explanation for why β declines with signal area that does not preclude the possibility that the maximum, i.e., whole-area signal condition is detected by a global linear integrator. He suggests that the visual system might employ linear filters matched in shape to the various signal-shape conditions. Thus for the single pie-wedge and windmill conditions these would be pie-wedge and windmill-shaped filters matched to the signal area, culminating in full-circle global linear integrators for the 100% signal area conditions.

Following the schematic of summation scenarios in Meese and Summers (2012), the matched filter model is illustrated in Figure 7, along with the "pure" PS model that we advanced previously and, for comparison, a "pure" linear summation model. For simplicity of exposition we will refer to the matched filter model simply as the "mixed" model, since it combines both linear filtering with PS across filter/stimulus positions. According to the mixed model, the decline in β with increasing signal area reflects the reduction in uncertainty as the matched filter grows to fill-up the stimulus area. Remember that with the pie-wedge shaped and windmill-shaped signals, their orientations were randomized on each stimulus presentation. This means that if we consider the matched filter as capturing all the signals in each signal-area condition, the number of nonsignal locations that the filter would likely sample, would decline with increasing signal area. From the point of view of the MAX-rule it means that the visual

Downloaded From: http://jov.arvojournals.org/pdfaccess.ashx?url=/data/Journals/JOV/934737/ on 12/08/2015

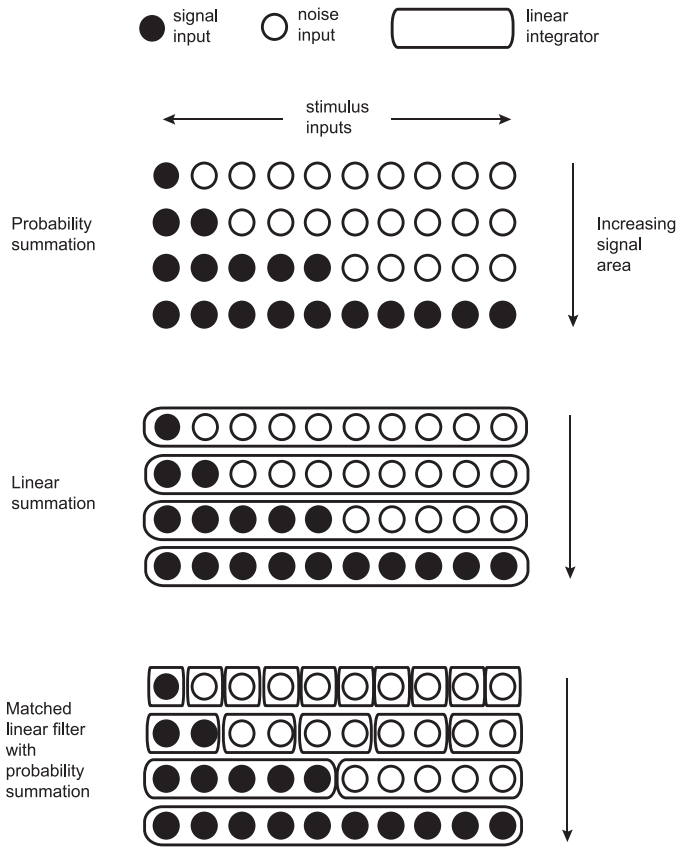

Figure 7. Three possible summation scenarios. The schematic follows that of figure 1 in Meese & Summers (2012). The filled black circles illustrate signal elements, whereas the empty circles illustrate noise elements. The bottom illustration illustrates the matched filter model (i.e., mixed model), where summation occurs over different groups of elements. See text for details.

system would examine independently each possible signal location with the matched filter and select the interval containing the maximum filter response. In terms of the SDT PS formulation described above, the relationships between Q (number of monitored channels or stimulus locations), n (number of signals), and signal area A are therefore different for the mixed compared to the pure PS model advanced above. In the pure PS model, Q is fixed and as signal area A is increases and so is n. In the matched filter model it works the other way round: as signal area A increases n remains fixed and Q declines.

We have applied the SDT PS formula to the mixed model situation. To understand how in principle the model can account for our results we begin with some reasonable assumptions. Throughout the modeling we assume an n of 1, that is, we consider the area containing the signal to stimulate a single matched filter, i.e., a single stimulus/channel. We define A, the area of the signal (and matched filter) as the percentage of total stimulus area. We then assume that each matched filter integrates N local samples from the stimulus, with N being equal to the area of the matched filter, i.e., ranging from 10 to 100. By "local samples" we mean local input signals with their own independent noise sources (see Figure 7). Finally, we assume that Q, which embodies the degree of uncertainty in the model, is equal to $100/A$, thus ranging from 10 to 1 as signal area increases from 10% to 100%. In other words, as the signal area and with it matched filter area increases, the number of nonsignal locations sampled on each trial by the matched filter, Q-1, declines proportionately.

To obtain the α-versus-A and β-versus-A slope predictions we use the PS formula in Equation 2, with n set to 1 and Q ranging from 10 to 1. Note that in the limiting case when $n = Q = 1$ Equation 2 reduces to the standard formula for calculating proportion correct for a single signal in an M-AFC task according to the MAX-rule under SDT (Kingdom & Prins, 2016). The linear summation component of the mixed model is achieved by computing for each condition $d' = (gs)^{\tau}\sqrt{N}$ with g (stimulus gain) and τ (transducer exponent) set to unity. A τ of 1 is the model value needed to produce the average β of 1.3 observed in the 100% signal area condition. The term $\sqrt{N}$ captures the fact that for a linear filter as N increases the amount of internal noise increases in proportion to the square root of the number of noise samples (because $N/\sqrt{N} = \sqrt{N}$). Psychometric functions of proportion correct as a function of stimulus strength s were then calculated for the 10 values of Q and fitted by Quick functions as described previously. The resulting α-versus-A and β-versus-A plots were then fitted as before by a straight line applied to the log–log data. The resulting slopes of the mixed model are −0.79 for α-versus-A and −0.184 for β-versus-A. These values are what one would expect from a mixed linear and PS model. The pure PS model predictions were −0.42 for the average α-versus-A slopes and −0.25 for average β-versus-A slopes. A pure linear summation model (under the fixed attention window scenario) would predict an α-versus-A slope of −1.0 and a β-versus-A slope of 0. The mixed model slopes therefore fall in between their corresponding pure probability and linear summation model values.

It is clear, however, that with the mixed model as it stands, the α-versus-A slope of −0.79 is too steep and the β-versus-A slope of −0.184 too shallow compared to the data, whose average values are −0.44 and −0.30, respectively. If we make N proportional to A^j and set j to 0.25 instead of 1.0, we can achieve an α-versus-A slope of −0.44. This would mean that the density of local samples integrated by the matched filter declines with the fourth root of the size of the filter, which to us seems implausible. Regarding the

Downloaded From: http://jov.arvojournals.org/pdfaccess.ashx?url=/data/Journals/JOV/934737/ on 12/08/2015

β-versus-A slope, its steepness is determined by the rate at which Q declines as a function of signal area, so it is clear that the mixed model rate of decline is insufficient to predict the data. However, it is not obvious to us what plausible mechanism would increase the rate of decline of Q with signal area. If rather than discretely positioning the matched filter on the available nonsignal location in order to tile the stimulus, the visual system performed a continuous convolution of the matched filter with the stimulus, i.e., "around the clock," this would presumably not increase the rate of Q decline, or if anything reduce it. Thus while the matched filter model is an important theoretical possibility, it does not appear to account for the data as well as the pure PS model advanced above, at least for the type of stimuli considered here.

Summary and conclusion

The main focus of this study was to test whether probability summation (PS) under signal-detection-theory (SDT) could be rejected as a model of signal integration in Glass pattern and Glass-pattern-like textures. We exploited one of the PS model's signature predictions: The exponent β of the psychometric functions should decrease as signal area is increased. Our results showed this characteristic, both in Glass patterns and Gabor textures. In addition, we found that the strength of summation across signal area was approximately half as strong as some previous reports. Moreover, we found no evidence for specialized detectors for circular textures; detection sensitivity was independent of texture type. Taken together, our findings show that probability *not* linear summation is the most likely basis for the detection of circular orientation-defined textures, and provide no support for the idea of specialized detectors for circular textures in vision.

Keywords: texture detection, glass pattern, global processing, probability summation, linear summation, additive summation, Signal Detection Theory, high threshold theory

Acknowledgments

This research was supported by the Australian Research Council (ARC) Discovery Project (Grant # DP110101511) given to JB and a Natural Sciences and Engineering Research Council of Canada grant #RGPIN 121713-11 given to FAAK.

Commercial relationships: none.

Corresponding author: Gunnar Schmidtmann; Frederick A. A. Kingdom.
Email: gunnar.schmidtmann@mcgill.ca; fred.kingdom@mcgill.ca.
Address: McGill Vision Research, Department of Ophthalmology, Montréal, Québec, Canada.

References

Achtman, R., Hess, R. F., & Wang, Y. Z. (2003). Sensitivity for global shape detection. *Journal of Vision*, *3*(10):4, 616–624, doi:10.1167/3.10.4. [PubMed] [Article]

Anzai, A., Peng, X., & Van Essen, D. C. (2007). Neurons in monkey visual area V2 encode combinations of orientations. *Nature Neuroscience*, *10*(10), 1313–1321.

Bell, J., & Badcock, D. R. (2008). Luminance and contrast cues are integrated in global shape detection with contours. *Vision Research*, *48*(21), 2336–2344.

Braddick, O. J., O'Brien, J. M., Wattam-Bell, J., Atkinson, J., & Turner, R. (2000). Form and motion coherence activate independent, but not dorsal/ventral segregated, networks in the human brain. *Current Biology*, *10*(12), 731–734.

Brainard, D. H. (1997). The Psychophysics Toolbox. *Spatial Vision*, *10*(4), 433–436.

Cadieu, C., Kouh, M., Pasupathy, A., Connor, C. E., Riesenhuber, M., Poggio, T., & Pasupathy, A. (2007). A model of V4 shape selectivity and invariance. *Journal of Neurophysiology*, *98*(3), 1733–1750.

Carandini, M., & Heeger, D. J. (2011). Normalization as a canonical neural computation. *Nature Reviews Neuroscience*, *13*, 51–62.

Dakin, S. C. (1997). The detection of structure in glass patterns: Psychophysics and computational models. *Vision Research*, *37*(16), 2227–2246.

Dakin, S. C., & Bex, P. J. (2002). Summation of concentric orientation structure: Seeing the Glass or the window? *Vision Research*, *42*(16), 2013–2020.

Desimone, R., Albright, T. D., Gross, C., & Bruce, C. (1984). Stimulus-selective properties of inferior temporal neurons in the macaque. *Journal of Neuroscience*, *8*(4), 2051–2062.

Dickinson, J., Harman, C., Tan, O., & Almeida, R. A. (2012). Local contextual interactions can result in global shape misperception. *Journal of Vision*,

Downloaded From: http://jov.arvojournals.org/pdfaccess.ashx?url=/data/Journals/JOV/934737/ on 12/08/2015

12(11):3, 1–20, doi:10.1167/12.11.3. [PubMed] [Article]

Dickinson, J. E., Broderick, C., & Badcock, D. R. (2009). Selective attention contributes to global processing in vision. *Journal of Vision*, *9*(2):6, 1–8, doi:10.1167/9.2.6. [PubMed] [Article]

Dickinson, J. E., Han, L., Bell, J., & Badcock, D. R. (2010). Local motion effects on form in radial frequency patterns. *Journal of Vision*, *10*(3)20, 1–15, doi:10.1167/10.3.20. [PubMed] [Article]

Dickinson, J. E., McGinty, J., Webster, K. E., & Badcock, D. R. (2012). Further evidence that local cues to shape in RF patterns are integrated globally. *Journal of Vision*, *12*(12):16, 1–17, doi:10.1167/12.12.16. [PubMed] [Article]

Dobbins, A., Zucker, S. W., & Cynader, M. S. (1987). Endstopped neurons in the visual cortex as a substrate for calculating curvature. *Nature*, *329*, 438–441.

Gallant, J. L., Connor, C. E., Rakshit, S., Lewis, J. W., & Van Essen, D. C. (1996). Neural responses to polar, hyperbolic, and Cartesian gratings in area V4 of the macaque monkey. *Journal of Neurophysiology*, *76*(4), 2718–2739.

Glass, L. (1969). Moiré effect from random dots. *Nature*, *223*, 578–580.

Glass, L., & Perez, R. (1973). Perception of random dot interference patterns. *Nature*, *246*, 360–362.

Goodale, M., & Milner, A. (1992). Separate visual pathways for perception and action. *Trends in Neuroscience*, *15*(1), 20–25.

Graham, N. (1989). *Visual pattern analyzers*. New York: Oxford University Press.

Green, D., & Swets, J. A. (1988). *Signal detection theory and psychophysics*. Huntington, New York: Krieger.

Hegdé, J., & Van Essen, D. C. (2007). A comparative study of shape representation in macaque visual areas V2 and V4. *Cerebral Cortex*, *17*(5), 1100–1116.

Hubel, D., & Wiesel, T. N. (1962). Receptive fields, binocular interaction and functional architecture in the cat's visual cortex. *Journal of Physiology*, *160*, 106–154.

Hubel, D. H., & Wiesel, T. N. (1968). Receptive fields and functional architecture of monkey striate cortex. *Journal of Physiology*, *195*(1), 215–243.

Kelly, D. M., Bischof, W. F., Wong-Wylie, D. R., & Spetch, M. L. (2001). Detection of glass patterns by pigeons and humans: Implications for differences in higher-level processing. *Psychological Science*, *12*(4), 338–342.

Kingdom, F. A. A., Baldwin, A. S., & Schmidtmann, G. (2015). Modeling probability and additive summation for detection across multiple mechanisms under the assumptions of signal detection theory. *Journal of Vision*, *15*(5):1, 1–16, doi:10.1167/15.5.1. [PubMed] [Article]

Kingdom, F. A. A., & Prins, N. (2016). *Psychophysics: A practical introduction* (2nd ed.). Academic Press, an imprint of Elseiver. (In press).

Kurki, I., Laurinen, P., Peromaa, T., & Saarinen, J. (2003). Spatial integration in Glass patterns. *Perception*, *32*(10), 1211–1220, doi:10.1068/p5102.

Kurki, I., & Saarinen, J. (2004). Shape perception in human vision: Specialized detectors for concentric spatial structures? *Neuroscience Letters*, *360*(1-2), 100–102.

Laming, D. (2013). Probability summation—A critique. *Journal of the Optical Society of America A*, *30*(3), 300–315.

Loffler, G. (2008). Perception of contours and shapes: Low and intermediate stage mechanisms. *Vision Research*, *48*(20), 2106–2127.

Loffler, G., Wilson, H. R., & Wilkinson, F. (2003). Local and global contributions to shape discrimination. *Vision Research*, *43*(5), 519–530.

Mayer, M. J., & Tyler, C. W. (1986). Invariance of the slope of the psychometric function with spatial summation. *Journal of the Optical Society of America A*, *3*(8), 1166–1172.

Meese, T. S., & Summers, R. J. (2012). Theory and data for area summation of contrast with and without uncertainty: Evidence for a noisy energy model. *Journal of Vision*, *12*(11):9, 1–28, doi:10.1167/12.11.9. [PubMed] [Article]

Meese, T. S., & Williams, C. B. (2000). Probability summation for multiple patches of luminance modulation. *Vision Research*, *40*(16), 2101–2113.

Morrone, M. C., Burr, D. C., & Vaina, L. M. (1995). Two stages of visual processing for radial and circular motion. *Nature*, *376*, 507–509.

Mullen, K., Beaudot, W., & Ivanov, I. V. (2011). Evidence that global processing does not limit thresholds for RF shape discrimination. *Journal of Vision*, *11*(3):6, 1–21, doi:10.1167/11.3.6. [PubMed] [Article]

Nachmias, J. (1981). On the psychometric function for contrast detection. *Vision Research*, *21*, 215–223.

Newsome, W. (1988). A selective impairment of motion perception following lesions of the middle temporal

Downloaded From: http://jov.arvojournals.org/pdfaccess.ashx?url=/data/Journals/JOV/934737/ on 12/08/2015

visual area (MT). *Journal of Neuroscience*, *8*(6), 2201–2211.

Or, C. C. F., & Elder, J. H. (2011). Oriented texture detection: Ideal observer modelling and classification image analysis. *Journal of Vision*, *11*(8):16, 1–20, doi:10.1167/11.8.16. [PubMed] [Article]

Ostwald, D., Lam, J. M., Li, S., & Kourtzi, Z. (2008). Neural coding of global form in the human visual cortex. *Journal of Neurophysiology*, *99*(5), 2456–2469, doi:10.1152/jn.01307.2007.

Pasupathy, A., & Connor, C. E. (1999). Responses to contour features in macaque area V4. *Journal of Neurophysiology*, *82*, 2490–2502.

Pasupathy, A., & Connor, C. E. (2002). Population coding of shape in area V4. *Nature Neuroscience*, *5*(12), 1332–1338.

Pei, F., Pettet, M. W., Vildavski, V. Y., & Norcia, A. M. (2005). Event-related potentials show configural specificity of global form processing. *NeuroReport*, *16*(13), 1427–1430.

Pelli, D. G. (1985). Uncertainty explains many aspects of visual contrast detection and discrimination. *Journal of the Optical Society of America A*, *2*(9), 1508–1531.

Pelli, D. G. (1997). The VideoToolbox software for visual psychophysics: Transforming numbers into movies. *Spatial Vision*, *10*(4), 437–442.

Prins, N., & Kingdom, F. A. A. (2009). Palamedes: Matlab routines for analyzing psychophysical data. Retrieved from http://www.palamedestoolbox.org

Quick, R. (1974). A vector-magnitude model of contrast detection. *Kybernetik*, *16*(2), 65–67.

Robson, J. G., & Graham, N. (1981). Probability summation and regional variation in contrast sensitivity across the visual field. *Vision Research*, *21*(3), 409–418.

Schmidtmann, G., Gordon, G. E., Bennett, D. M., & Loffler, G. (2013). Detecting shapes in noise: tuning characteristics of global shape mechanisms. *Frontiers in Computational Neuroscience*, *7*(37), 1–14.

Schmidtmann, G., Kennedy, G. J., Orbach, H. S., & Loffler, G. (2012). Non-linear global pooling in the discrimination of circular and non-circular shapes. *Vision Research*, *62*, 44–56.

Serre, T., Kouh, M., Cadieu, C., Knoblich, U., Kreiman, G. & Poggio, T. (2005). A Theory of Object Recognition: Computations and Circuits in the Feedforward Path of the Ventral Stream in Primate Visual Cortex. *AI Memo 2005–036/CBCL Memo 259*. Cambridge, MA: MIT.

Serre, T., Oliva, A., & Poggio, T. (2007). A feedforward architecture accounts for rapid categorization. *Proceedings of the National Academy of Sciences, USA, 104*(15), 6424–6429.

Seu, L., & Ferrera, V. P. (2001). Detection thresholds for spiral Glass patterns. *Vision Research*, *41*(28), 3785–3790.

Shimozaki, S. S., Eckstein, M. P., & Abbey, C. K. (2003). An ideal observer with channels versus feature-independent processing of spatial frequency and orientation in visual search performance. *Journal of the Optical Society of America A*, *20*(12), 2197–2215.

Smith, M. A., Bair, W., & Movshon, J. A. (2002). Signals in macaque striate cortical neurons that support the perception of glass patterns. *Journal of Neuroscience*, *22*(18), 8334–8345.

Smith, M. A., Kohn, A., Movshon, J. A., & Movshon, J. A. (2007). Glass pattern responses in macaque V2 neurons. *Journal of Vision*, *7*(3):5, 1–15, doi:10.1167/7.3.5. [PubMed] [Article]

Strasburger, H. (2001). Converting between measures of slope of the psychometric function. *Perception and Psychophysics, 63*(8), 1348–1355, http://doi.org/10.3758/BF03194547.

Tan, K. W. S., Bowden, V. K., Dickinson, J. E., & Badcock, D. R. (2015). Modulated textures with shape structures implied by a closed flow are processed globally. *Journal of Vision*, *15*(3):17, 1–18, doi:10.1167/15.3.17. [PubMed] [Article]

Tan, K. W. S., Dickinson, J. E., & Badcock, D. R. (2013). Detecting shape change: Characterizing the interaction between texture-defined and contour-defined borders. *Journal of Vision*, *13*(14):12, 1–16, doi:10.1167/13.14.12. [PubMed] [Article]

Tanaka, K. (1996). Inferotemporal cortex and object vision. *Annual Review of Neuroscience*, *19*(1), 109–139.

Tsao, D. Y., & Livingstone, M. S. (2008). Mechanisms of face perception. *Annual Review of Neuroscience*, *31*, 411–437.

Tyler, C. W., & Chen, C.-C. (2000). Signal detection theory in the 2AFC paradigm: Attention, channel uncertainty and probability summation. *Vision Research*, *40*, 3121–3144.

Ungerleider, L. G., & Mishkin, M. (1982). Two cortical visual systems. In D. J. Ingle, M. A. Goodale, & R. J. W. Mansfield (Eds.), *Analysis of visual behavior* (pp. 549–586). Cambridge, MA: MIT Press.

Van Essen, D., Anderson, C., & Felleman, D. (1992). Information processing in the primate visual system: An integrated systems perspective. *Science*, *255*(5043), 419–423.

Downloaded From: http://jov.arvojournals.org/pdfaccess.ashx?url=/data/Journals/JOV/934737/ on 12/08/2015

Watson, A. B. (1979). Probability summation over time. *Vision Research*, *19*, 515–522.

Wilson, H., Wilkinson, F., & Asaad, W. (1997). Concentric orientation summation in human form vision. *Vision Research*, *37*(17), 2325–2330.

Wilson, H. R. (1999). Non-Fourier cortical processes in texture, form, and motion perception. In P. S. Ulinski & E. G. Jones (Eds.), *Cerebral Cortex, 13: Models of cortical circuitry* (pp. 445–477). New York: Plenum.

Wilson, H. R., & Wilkinson, F. (1998). Detection of global structure in Glass patterns: Implications for form vision. *Vision Research*, *38*, 2933–2947.

Wilson, H. R., & Wilkinson, F. (2015). From orientations to objects: Configural processing in the ventral stream. *Journal of Vision*, *15*(7):4, 1–10, doi: 10.1167/15.15.4. [PubMed] [Article]

Yau, J., Pasupathy, A., Brincat, S., & Connor, C. E. (2012). Curvature processing dynamics in macaque area V4. *Cerebral Cortex*, *23*(1), 198–210.

Downloaded From: http://jov.arvojournals.org/pdfaccess.ashx?url=/data/Journals/JOV/934737/ on 12/08/2015